Experimental Investigation of the Air Exchange Effectiveness of Push-Pull Ventilation Devices

Sven Auerswald [1],*[iD] **, Carina Hörberg** [1]**, Thibault Pflug** [1]**, Jens Pfafferott** [2]**, Constanze Bongs** [1] **and Hans-Martin Henning** [1][iD]

[1]   Fraunhofer Institute for Solar Energy Systems ISE, 79110 Freiburg, Germany
[2]   Institute of Energy Systems Technology (INES), Faculty of Mechanical and Process Engineering, Offenburg University of Applied Sciences, 77652 Offenburg, Germany
*   Correspondence: sven.auerswald@ise.fraunhofer.de

check for updates

Abstract: The increasing installation numbers of ventilation units in residential buildings are driven by legal objectives to improve their energy efficiency. The dimensioning of a ventilation system for nearly zero energy buildings is usually based on the air flow rate desired by the clients or requested by technical regulations. However, this does not necessarily lead to a system actually able to renew the air volume of the living space effectively. In recent years decentralised systems with an alternating operation mode and fairly good energy efficiencies entered the market and following question was raised: "Does this operation mode allow an efficient air renewal?" This question can be answered experimentally by performing a tracer gas analysis. In the presented study, a total of 15 preliminary tests are carried out in a climatic chamber representing a single room equipped with two push-pull devices. The tests include summer, winter and isothermal supply air conditions since this parameter variation is missing till now for push-pull devices. Further investigations are dedicated to the effect of thermal convection due to human heat dissipation on the room air flow. In dependence on these boundary conditions, the determined air exchange efficiency varies, lagging behind the expected range $0.5 < \varepsilon^a < 1$ in almost all cases, indicating insufficient air exchange including short-circuiting. Local air exchange values suggest inhomogeneous air renewal depending on the distance to the indoor apertures as well as the temperature gradients between in- and outdoor. The tested measurement set-up is applicable for field measurements.

Keywords: decentralised ventilation; ventilation effectiveness; air exchange efficiency; push-pull

1. Introduction

Construction tasks in Europe are increasingly focusing on the maintenance and refurbishment of existing buildings. Legislative and technical regulations in Europe and Germany require buildings with an improved airtightness of their envelope. Due to these requirements the installation of mechanical ventilation systems is becoming a common practice in residential buildings. As a result in Germany especially decentralised systems gain a continuously growing market share as it is obvious in Figure 1 [1–4]. But, while regulations focus on the energy efficiency of these systems residents prefer silent and energy efficient ventilation systems providing the required amount of fresh air [5]. Out of these three aspects the last one is most important for residents.
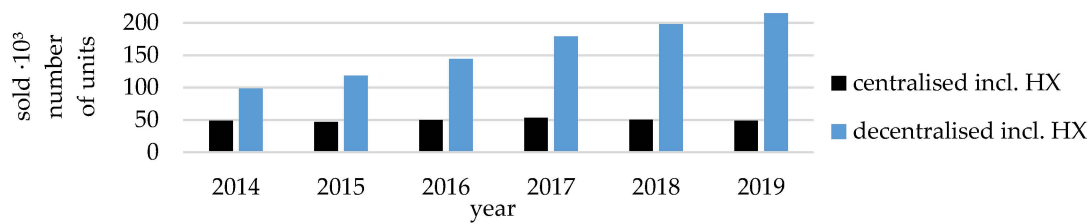
Figure 1. Market development of ventilation systems in Germany; HX = heat exchanger [1–4].

1.1. Push-Pull Ventilation Devices

Façade-integrated, regenerative and decentralised ventilation devices, operating in alternating mode (push-pull devices) are interesting both for new buildings and renovation. Based on a short market research of 31 push-pull devices available in Germany an average device has the characteristics according to Table 1. As no ductwork is required and the installation is simple, with only a core-hole and electrical connections needed, they initially seem superior in comparison to central systems from a business-economic point of view [6].

Table 1. Average "data sheet" of push-pull devices based on 31 devices available for the German market [7].

Characteristic	Value	Uncertainty ($k_p = 2$)
Specific energy consumption class	B to A+	
Thermal efficiency	85%	±13%
Electrical power input		
Maximum	10 W	±18 W
Minimum	3 W	±3 W
Volume flow		
Maximum	$46 \, \mathrm{m^3 \cdot h^{-1}}$	$\pm 34 \, \mathrm{m^3 \cdot h^{-1}}$
Minimum	$17 \, \mathrm{m^3 \cdot h^{-1}}$	$\pm 15 \, \mathrm{m^3 \cdot h^{-1}}$
Specific power input	$0.23 \, \mathrm{W \cdot h \cdot m^{-3}}$	$\pm 0.19 \, \mathrm{W \cdot h \cdot m^{-3}}$
Sound power level		
Maximum	37 dB(A)	±13 dB(A)
Minimum	22 dB(A)	±11 dB(A)
Acoustic insulation from the outside	43 dB(A)	±20 dB(A)
Geometry		
Hydraulic diameter of the wall opening	194 mm	±123 mm
Minimal wall thickness	266 mm	±164 mm
Filter	G3/G4 optional F7/F8	
Controller input	if available : φ_{in} (or C_{in})	

1.1.1. Principle of Operation and Its Consequences

The simplest push-pull ventilation system consists out of one pair of those devices as depicted by Figure 2. The regenerative heat exchangers are activated through the alternating operation mode where one device always operates in the opposite flow direction of the other.

After a typically constant time interval of ~60 s the alternation of the phases takes place. This way the heat exchangers are charged and discharged in a constantly successive changes. This alternating operation mode has an impact on the flow pattern in the living space and the devices themselves as well. One weak point of these devices is that they have always a certain ventilation short-cut during the transition from one phase to the other. This is because of the air volume left inside the devices just before the transition. Another thing is their vulnerability towards pressure differences between in- and outside. This is because most of the devices use an axial fan to perform the reversal of the flow direction.
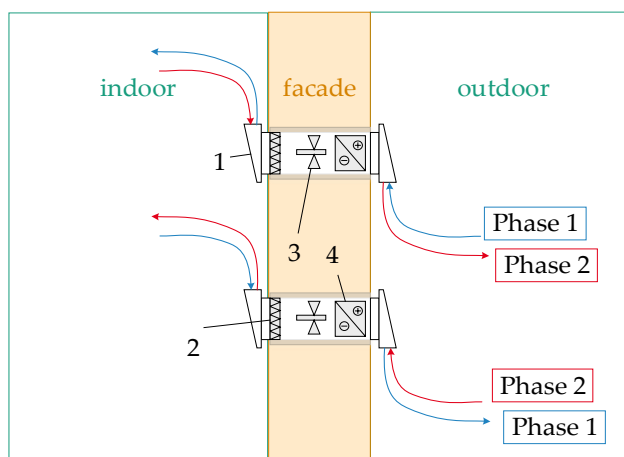
Figure 2. Sketch of a pair of push-pull ventilation devices; (1) aperture, (2) filter, (3) axial fan, (4) regenerative heat exchanger.

1.1.2. Literature Review: Air Exchange Efficiency

An early publication by Manz et al. regarding the air exchange efficiency of decentralized devices presented results with air exchange efficiency ε^a for push-pull devices as high as 0.83. However, in the case which resulted in such high efficiencies the setup included heat sources with up to 325 W [6]. Merzkirch compared push-pull devices with decentralized and centralized continuous flow ventilations systems both during field tests and in a CFD-simulation. He found that decentralized devices fall short in air exchange efficiency compared to centralized devices, the measurements even came to the result that decentralized devices may lead to ventilation short-cuts ($\varepsilon^a < 0.50$) [8]. Another publication regarding push-pull devices has been released by three German research institutes and the German professional association for buildings and indoor climate [9]. In that study they addressed a further development of the current technical regulations (especially DIN 1946-6 [10]), improved measurement techniques for the volume flow and the energy efficiency of push-pull devices as well as a CFD-analysis of flats and buildings equipped with push-pull devices. Similar scientific work on rooms and flats equipped with push-pull devices, summarized in Table 2, indicate that the global air exchange efficiency ε^a is close to ideal mixing ($\varepsilon^a = 0.50$).

Table 2. Literature review of global air exchange efficiencies ε^a, according to Equation (6), in rooms equipped with push-pull device.
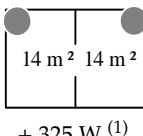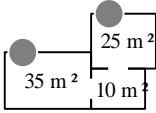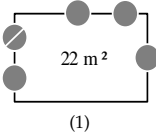
Ref.	System	Boundary Conditions		Method	ε^a
[6]	14 m² 14 m² + 325 W (1)	Unit $\dot{V}$ t_{cyc} $\Delta_{oi}\bar{\vartheta}$	Lüftungstechnik Meinerzhagen $= 50\,m^3 \cdot h^{-1}$ alternating $= 80\,s$ $= [-24, -11]\,K$	LM (4) tracer gas : SF_6	[0.63, 0.83]
[8]	60 m² … 110 m²	Unit $\dot{V}$ t_{cyc} $\Delta_{oi}\bar{\vartheta}$	Lunos e² [11] $= [18, 31]\,m^3 \cdot h^{-1}$ alternating $= 70s$ n.a.	FM (5) tracer gas : $C_2H_2F_4$ (R134a)	[0.45, 0.48]
[8]	60 m² … 110 m²	Unit $\dot{V}$ t_{cyc} $\Delta_{oi}\bar{\vartheta}$	LTM Thermolüfter 1230 $= [12.5, 65]\,m^3 \cdot h^{-1}$ alternating $= 50\,s$ n.a.	FM (5) tracer gas : $C_2H_2F_4$ (R134a)	[0.38, 0.47]

Table 2. *Cont.*

Ref.	System	Boundary Conditions		Method	ε^a
[8]	25 m² 35 m² 10 m²	Unit $\dot{V}$ t_{cyc} $\Delta_{oi}\overline{\vartheta}$	n.a. $= 30\ \mathrm{m^3 \cdot h^{-1}}$ alternating n.a. n.a.	CFD	0.55
[9]	22 m² (1)	Unit $\dot{V}$ t_{cyc} $\Delta_{oi}\overline{\vartheta}$	n.a. $\approx 43\ \mathrm{m^3 \cdot h^{-1}}^{(2),(3)}$ n.a. $= -13\ \mathrm{K}$	CFD	[0.49, 0.55]
[12]	n.a.	Unit $\dot{V}$ t_{cyc} $\Delta_{oi}\overline{\vartheta}$	Renson Endura Twist $= 30\ \mathrm{m^3 \cdot h^{-1}}$ $= 30\ \mathrm{s}$ $= -20\ \mathrm{K}$	LM [4] tracer gas : CO_2	0.53
[12]	n.a.	Unit $\dot{V}$ t_{cyc} $\Delta_{oi}\overline{\vartheta}$	O.ERRE Tempero eco 150 ceram n.a. $= 70\ \mathrm{s}$ $= -20\ \mathrm{K}$	LM [4] tracer gas : CO_2	0.51

[1] Various balanced systems, [2] nominal ventilation according to [10], [3] Twin-devices: two push-pull devices in one casing (filled circle + diagonal line), [4] LM = lab measurement, [5] FM = field test measurement.

However, the previously presented results show as well that ε^a is sometimes below 0.50, which is a hint for ventilation short-cuts. Furthermore, until now there is no significant amount of data available to clearly state whether push-pull devices provide fresh air with sufficient air exchange efficiency, and under which conditions this statement it is valid. To generate such data it is helpful to reduce caveats from the residents towards the measurement set-up, reduce investment costs for the set-up and reduce the effort to generate the results. This way campaigns in existing buildings, equipped with push-pull devices, are more likely. Additionally, there is just one laboratory study and no field measurement available, which applies CO_2 as a tracer gas for the air exchange effectiveness evaluation of push-pull devices. This is relevant since CO_2 has several advantages over other tracer gases most importantly its low health risks, its density compared to air and its low costs [13].

1.2. Aim of this Study

Within the scope of this study, an approach to measure the ventilation effectiveness of push-pull devices in a laboratory is presented. The method is adaptable to the wide diversity of situations in the field. This first measurement campaign aims to check if a low cost tracer-gas set-up based on CO_2, accepted by residents in their living space and with several sensors per room can generate a sufficient data quality to evaluate the global and local air exchange efficiency.

A second aim is to apply the method to a laboratory test case to investigate whether the available push-pull devices distribute the fresh air flow efficiently throughout the whole living space, under different sets of boundary conditions. This preliminary study shall therefore lead to an estimation if it is necessary to evaluate the ventilation effectiveness under varying outdoor climate conditions or if the focus of the indoor boundary conditions is sufficient for such a study.

2. Materials and Methods

2.1. Theory: Ventilation Effectiveness

The primary goal of ventilation is to provide fresh air while removing internally produced pollutant loads. The indicators for assessing ventilation effectiveness can be divided into two categories listed in Table 3. The informative value of the indicators can vary depending on the situation. With known

location and intensity of the pollutant source the evaluation of contaminant removal indicators provide meaningful results. For cases in which no or just limited information on the pollutant source is available the evaluation of air renewal assessment parameters is more suitable.

Table 3. Nomenclature of ventilation effectiveness.

Evaluation of Contaminant Removal		Evaluation of Air Renewal	
(Global) ventilation efficiency	ε^c	(Global, absolute) air exchange efficiency	ε^a
Local ventilation efficiency	ε_i^c	(Nominal relative) local air exchange index	ε_i^a
		(Relative) local air exchange indicator	$\varepsilon_{N,j}^a$

2.1.1. Age of Air

The age of air τ introduced by Sandberg [14] is an important instrument to analyse ventilation effectiveness. It defines the time that has elapsed between the entry of fresh air into a building zone until its reaching of a specific point i in that same zone. For an ideal piston flow the local age of air $\overline{\tau}_{P,i}$ may be interpreted as the time it takes an imaginary piston starting from the side of the room to reach a certain point. The growth is linear from $\tau_{sup} = 0$ to τ_{exh} at the air exhaust opening. As the piston flow crosses the space in the most direct way, the local age of air at the outlet simultaneously represents the shortest theoretically possible residence time of air in any room. It is called nominal air age τ_{nom} and defined by Equation (1), where V is the volume ventilated and $\dot{V}$ is the effective ventilation volume flow. The reciprocal of τ_{nom} is the nominal air-exchange rate n_{nom} [14]. For the special case of a piston flow $\tau_{exh} = \tau_{nom}$.

$$\tau_{nom} = \frac{V}{\dot{V}} = \frac{1}{n_{nom}}, \tag{1}$$

However, in most cases of rooms in real buildings there is no air flow similar to piston flow. The flow is rather turbulent and not directed from the entry to the exhaust. Furthermore, the flow is not distributed evenly in the room cross-section. The local air age of each coordinate in a room can be evaluated by the methods described by Sandberg [14] and ISO 16000-8 [15]. All of these methods are based on time dependent measurements of a tracer gas concentration $C(t)$ at specific spatial coordinates in the room (P, i). The most popular method is the concentration decay method. For this method the air age of a coordinate i is calculated by approximating Equation (2) with the compound trapezoidal rule by Goodwin [16] according to ISO 16000-8 [15] or Mundt et al. [17]. Furthermore, the outdoor concentration of CO_2 has to be considered through the mass balance of CO_2 and the following assumptions [13].

1. The density of unsaturated moist air is constant for the entire measurement time interval and volume: $\rho_{ma}(\varphi < 1) = \text{const.} \; \forall t \in [t_0, \, t_f] \; \wedge \; \forall x \in V$
2. The molar mass of unsaturated moist air is constant for the entire measurement time interval and volume: $M_{ma}(\varphi < 1) = \text{const.} \; \forall t \in [t_0, \, t_f] \; \wedge \; \forall x \in V$
3. The volume flow is constant for the entire measurement time interval: $\overline{\dot{V}}(t) = \dot{V}_{sup}(t) = \dot{V}_{exh}(t) = \text{const.} \; \forall t \in [t_0, \, t_f]$
4. The outdoor/background CO_2-concentration is constant for the entire measurement time interval: $C_{out}(t) = \text{const.} \; \forall t \in [t_0, \, t_f]$

The initialization time t_0 is the removal of the taped piece of cardboard on the outdoor apertures of the push-pull devices. As termination criterion served Equation (3), which represents the undercut of 37% of the concentration difference between absolute initial and natural background

concentration [18,19]. With the initial and the termination concentration and time the residual tail parameter λ_{tail} for the approximation of $\overline{\tau}_{P,i}$ has been calculated according to Equation (4).

$$\overline{\tau}_{P,i} \;=\; \frac{1}{\Delta C_{P,i}(t=t_0)} \cdot \int_{\infty}^{t_0} \Delta C_{P,i}(t)dt, \; \text{with } \Delta C_{P,i}(t) = C_{P,i}(t) - C_{out} \tag{2}$$

$$\Delta C_{P,i}(t_f) \;<\; 37\% \;\cdot\; \Delta C_{P,i}(t_0) \tag{3}$$

$$\lambda_{tail} = \ln\!\left(\frac{\Delta C_{P,i}(t_f)}{\Delta C_{P,i}(t_0)}\right) \cdot \frac{1}{t_0 - t_f} \tag{4}$$

The spatial average of air age $\langle\overline{\tau}\rangle$ is given by Equation (5), where N is the number of considered measurements points.

$$\langle\overline{\tau}\rangle \;=\; \frac{\sum_{i=1}^{N} \overline{\tau}_{P,i}}{N} \;=\; \frac{1}{\langle\overline{n}\rangle}, \tag{5}$$

This approach by Sandberg [20] has been used instead of the definition like in [17] or [21], which is based on tracer gas concentrations in the exhaust ducts. The presented approach is favoured here since of the alternating behaviour of the duct concentrations.

2.1.2. Global Absolute Air Exchange Efficiency

To evaluate the global absolute air exchange efficiency ε^a the definition of Equation (6) has been applied [22,23]. As a result, ε^a is a global parameter of a considered air volume, which compares the current real behaviour described by $\langle\overline{n}\rangle$ to the corresponding theoretical maximum value $2 \cdot n_{nom}$.

$$\varepsilon^a \;=\; \frac{\tau_{nom}}{2} \cdot \frac{1}{\langle\overline{\tau}\rangle} \;=\; \frac{1}{2} \cdot \frac{\langle\overline{n}\rangle}{n_{nom}}, \tag{6}$$

The room average age of air $\langle\overline{\tau}\rangle$ reaches its lowest value for ideal piston flow. The resulting global air exchange efficiency of $\varepsilon^a = 100\%$ represents the upper limit. For ideal mixing ventilation (usual assumption for most indoor air studies), a homogeneous age of air $\overline{\tau}_{P,i} = $ const. $\forall i \in \mathbb{N}^*$ is assumed throughout the room. This results in $\varepsilon^a = 50\%$, which characterises an even distribution of new and old air throughout the whole room. Compared to an ideal piston flow this state is reached when the "piston" has travelled half way through the room [22]. The global air exchange efficiency in well operating ventilation systems should reach a value between these two reference values $\varepsilon^a = [50, 100]\%$. Lower efficiencies indicate short-circuit currents and stagnating areas.

2.1.3. Local Air Exchange

For the evaluation of the situation at a point i in a room, both Novoselac [23] and Mundt et al. [17] mention the local air exchange index ε_i^a according to Equation (7). This index provides a parameter which compares the local air age $\overline{\tau}_{P,i}$ in the room with the global design parameter nominal air age τ_{nom}. Therefore, it is depends on the knowledge of the ventilation volume flow rate $\dot{V}$ and the volume to be ventilated V. Both measures can be difficult to evaluate in practice. In case of ideal mixing or an even better air exchange all ε_i^a are equal to or larger than 1 ($\varepsilon_i^a \geq 1 \; \forall i \in \mathbb{N}^*$). Since, ideal mixing means an even distribution of old and new air throughout the whole volume the Range $R_{\varepsilon_i^a} = \left| \min(\varepsilon_i^a) - \max(\varepsilon_i^a) \right|$ of all ε_i^a should approach to 0 ($\lim_{i\to\infty} R_{\varepsilon_i^a} = 0 \; \forall i \in \mathbb{N}^*$), additionally.

$$\varepsilon_i^a \;=\; \frac{\tau_{nom}}{\overline{\tau}_{P,i}}, \tag{7}$$

However, ε_i^a does not relate to the spatial average room age of air $\langle\overline{\tau}\rangle$, therefore it is not unambiguously evident whether zones of the room are ventilated above or below spatial average. More importantly the volume flow $\dot{V}$ of the push-pull devices has a considerable range of uncertainty.

This is because their alternating volume flow is always transient with a defined period time. Furthermore, push-pull devices are known for their vulnerability to pressure differences due to wind or additional exhaust only devices. Therefore, the local air exchange indicator $\varepsilon_{N,j}^a$ by Skaaret [22] according to Equation (8) is additionally used in this paper.

$$\varepsilon_{N,j}^a = \frac{\langle\overline{\tau}\rangle}{\overline{\tau}_{P,j}}, \tag{8}$$

In case of ideal mixing, the air ages τ_{nom}, $\langle\overline{\tau}\rangle$ and $\overline{\tau}_P$ are all equal and the Equations (7) and (8) always deliver 1. For other cases, the values vary depending on the spatial position and the ratio between τ_{nom} and $\langle\overline{\tau}\rangle$. If the local age of air at any point j in the room ($\overline{\tau}_{P,j}$) is different than the average of all local ages of air in the room $\langle\overline{\tau}\rangle$, the resulting air exchange indicators are $\varepsilon_{N,j}^a \neq 1 \; \forall j \in \mathbb{N}^*$. Values $\varepsilon_{N,j}^a > 1$ indicate better ventilated areas with $\overline{\tau}_P < \langle\overline{\tau}\rangle$. Since, in case of ideal mixing $\overline{\tau}_{P,i} = $ const. $\forall i \in \mathbb{N}^*$ the range $R_{\varepsilon_{N,j}^a}$ of all $\varepsilon_{N,j}^a$ should approach to 0 ($\lim_{j\to\infty} R_{\varepsilon_{N,j}^a} = 0 \; \forall j \in \mathbb{N}^*$) as well. Important to understand is that results of $\varepsilon_{N,j}^a$ are strongly depended on the distribution of the sensors used to calculate $\langle\overline{\tau}\rangle$. To get a good reference value for the spatial average of air age $\langle\overline{\tau}\rangle$ the sensor positions i should be well or better evenly distributed over the volume to be evaluated.

2.2. Methodology of the Measurements

2.2.1. Investigated Ventilation Units

The units investigated are push-pull devices (Lunos e^2). An axial fan inside the unit delivers a maximum air flow of 15 m$^3\cdot$h^{-1} in the first level and 30 m$^3\cdot$h^{-1} in a second level. The flow direction is reversed every 70 seconds. During the exhaust air phase, the regenerative heat exchanger is charged with thermal energy of the room air in order to subsequently heat the incoming supply air.

2.2.2. Experimental Setup

The investigations are carried out in a full-scale inner climatic chamber (ICC) of 2.77 m × 2.70 m × 5.00 m that is connected to an external climatic chamber (ECC) at the Institute of Energy Systems Technology (INES) of Offenburg University of Applied Sciences. A passive-house insulated façade with one window and two push-pull devices each to the right and left of it (clear distance 1.35 m) is integrated into the 4 m^2 opening between ICC and ECC [24]. A short description of the relevant measurements are given by Table 4.

Table 4. Short description of the measurements performed.

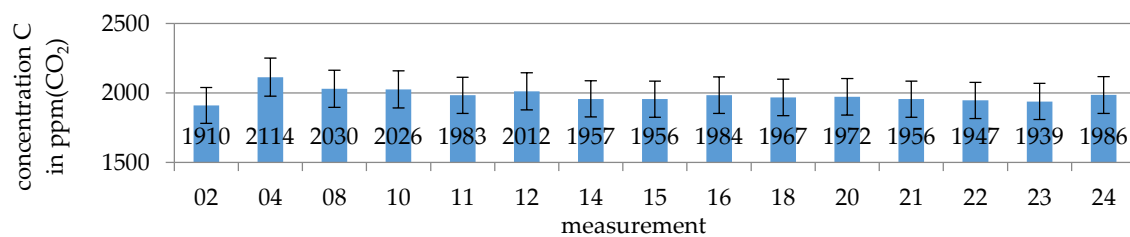| #	Description
2	$\dot{V}$ = 28 m$^3\cdot$h^{-1}, isotherm, horizontal plane: 2.2 m
4	$\dot{V}$ = 15 m$^3\cdot$h^{-1}, isotherm, horizontal plane: 2.2 m
8	$\dot{V}$ = 28 m$^3\cdot$h^{-1}, isotherm, horizontal plane: 1.1 m
10	$\dot{V}$ = 15 m$^3\cdot$h^{-1}, isotherm, horizontal plane: 1.1 m
11	$\dot{V}$ = 28 m$^3\cdot$h^{-1}, winter, horizontal plane: 1.1 m
12	$\dot{V}$ = 28 m$^3\cdot$h^{-1}, winter, horizontal plane: 2.2 m
14	$\dot{V}$ = 28 m$^3\cdot$h^{-1}, summer, horizontal plane: 2.2 m
15	$\dot{V}$ = 15 m$^3\cdot$h^{-1}, summer, horizontal plane: 2.2 m
16	$\dot{V}$ = 15 m$^3\cdot$h^{-1}, summer, horizontal plane: 1.1 m
18	$\dot{V}$ = 28 m$^3\cdot$h^{-1}, summer, horizontal plane: 1.1 m
20	$\dot{V}$ = 15 m$^3\cdot$h^{-1}, isotherm + dummy, horizontal plane 1.1 m
21	$\dot{V}$ = 15 m$^3\cdot$h^{-1}, winter, horizontal plane: 1.1 m
22	$\dot{V}$ = 15 m$^3\cdot$h^{-1}, winter, horizontal plane: 2.2 m
23	$\dot{V}$ = 28 m$^3\cdot$h^{-1}, isotherm + dummy, horizontal plane: 2.2 m
24	$\dot{V}$ = 28 m$^3\cdot$h^{-1}, isotherm + dummy, horizontal plane: 1.1 m

Initially, the air of the ICC corresponds to the conditions of the surrounding laboratory and is neither heated nor (de)humified in the experimental setup. In the following the influence of the various thermal conditions is investigated. Conditions subject to analysis are (a) the case in which temperatures in the indoor and outdoor chamber are unaffected and thus similar (called isothermal: $\vartheta_{ECC} \approx \vartheta_{ICC}$, no heat regeneration occurs), (b) summer and (c) winter conditions in the ECC. The effect of these different boundary conditions on the indoor air (ICC) distribution is examined. For emulated summer conditions the supply air to the ECC is heated with fan heaters. In contrast to that cold air from the vicinity of the laboratory building is used to create emulated winter conditions. All hygrothermal boundary conditions established during the measurements are summarized Table 5. In a further step, a heat load dummy (300 W) is placed halfway between the façade equipped with push-pull devices and the opposite room wall in order to represent the heat dissipation of two adults. To evaluate air exchange efficiency, the concentration decay method is carried out. For this CO_2 is accumulated in the ICC until $\approx$ 2000 ppm according to the definition in Equation (9). This considers a mean concentration for each sensor of a full push-pull ventilation cycle (140 s). The initial mean concentration of all sensors varied between one and another decay measurement within the interval of [1910, 2114] ppm and are summarized in Figure 3. The range between the maximum and minimum mean initial concentration of the sensors used to be smaller than $R_c <$ 250 ppm.

$$\frac{1}{N} \cdot \sum_{i=1}^{N} \left(\frac{1}{N_i} \cdot \sum_{t=t_0-140\,s}^{t_0} C_{P,i}(t) \right) \approx 2\,000 \text{ ppm,}$$

$$\forall i \in \mathbb{N}^* \ \wedge \ N_i = \left| \{ C_{P,i}(t) \middle| \in [t_0 - 140\,s, t_0] \} \right| \ \wedge \ N = \left| \{ \text{active sensor positions} \} \right| \tag{9}$$

Table 5. Hygrothermal conditions in external climatic chamber (ECC) over 4 measurements each.

Condition	Temperature ϑ_{ECC} in °C	ϑ-range R_ϑ in °C	Abs. Humidity $\overline{X}_{ECC}$ in g(H$_2$O)·kg(da)$^{-1}$	X-range R_X in g(H$_2$O)·kg(da)$^{-1}$
Isothermal	22.1	3.2	4.9	3.6
Summer	36.9	10.5	4.2	2.9
Winter	8.3	7.6	4.0	1.8

Figure 3. Initial concentrations including simple uncertainty error bars.

These relatively low initial concentration levels are chosen based on the lowest upper measurement limit (2000 ppm) of the sensors available for the campaign. ISO 16000-8 recommends an initial concentration of 100· detection limit, which would be equal to $\approx$ 5000 ppm [15]. To homogenise the accumulating CO_2 circulation fans have been placed in the ICC, which can be switched off remotely without entering the ICC. For the injection of the CO_2 into the ICC a hose connected to a pressurised gas cylinder outside the ICC has been used. During the homogenisation the outside apertures of the push-pull devices are blocked by cardboard caps. The devices are then switched on during the homogenisation. The initialisation of the decay measurement is the removal of the cardboard caps. Sensors at max(N) = 17 positions shown in Figure 4 and summarized in Table 6 record the discharging behaviour of the employed tracer gas.

Table 6. Sensor positions, uncertainties and rages.

| Pos.	x, in m	y, in m	z, in m	Measured Quantities	Sensors
MP01	0.10	1.35	2.35	C, φ, ϑ u, ϑ	Testo CO_2 probe ONr. 0632 1240 [25] Testo humidity sensor ONr. 0636 9740 [26] Testo turbulence probe ONr. 0628 0009 [27]
MP02	0.60	1.35	2.35	C, φ, ϑ	Testo CO_2 probe ONr. 0632 1240 [25] Thermokon SR65 rH [28]
MP03	1.10	1.35	2.35	C, φ, ϑ u, ϑ	Testo CO_2 probe ONr. 0632 1240 [25] Testo humidity sensor ONr. 0636 9743 [29] Testo turbulence probe ONr.0628 0009 [27]
MP04	1.70	1.35	2.35	C, φ, ϑ u, ϑ	Testo IAQ probe ONr. 0632 1543 [30] Testo turbulence probe ONr. 0628 0143 [31]
MP05	2.00	0.70	4.70	C, φ, ϑ u, ϑ	Testo IAQ probe ONr. 0632 1543 [30] Testo turbulence probe ONr. 0628 0143 [31]
MP06	2.00	2.00	4.70	C, φ, ϑ u, ϑ	Testo IAQ probe ONr. 0632 1543 [30] Testo turbulence probe ONr. 0628 0143 [31]
MP06e	ECC push-pull right			C, φ, ϑ	Testo IAQ probe ONr. 0632 1543 [30]
MP07	2.25	1.35	2.35	C	
MP08	2.25	0.50	2.35	C	
MP09	2.25	0.50	0.50	C	
MP11	2.25	2.20	4.20	C	
MP12	2.25	0.85	4.20	C	
MP14	1.10	0.50	0.50	C	
MP15	1.10	2.20	0.50	C	Afriso CO2-Sensor F [32]
MP16	1.10	1.35	1.45	C	
MP17	1.10	1.35	3.35	C	
MP18	1.10	0.85	4.20	C	
MP19	1.10	0.85	4.20	C	
MP21e	ECC window			C	
MP22e	ECC push-pull left			C	
MP05i	2.00	0.70	4.70	C	

C: CO_2-concentration in ppm, φ: relative humidity in %rh, ϑ: temperature in °C, u: air velocity in m·s^{-1}; ONr: Testo Order-Number. The uncertainty of the sensors is detailed in Section 2.2.3 All sensors have been calibrated. The CO_2 ranges are for Afriso [0,2000] ppm and for Testo [0,10,000] ppm.

Because of a limitation in the number of sensors experiments with the same volume flow settings and hygrothermal boundary conditions are done twice in order to measure two horizontal planes at ~1.10 m (sensors: 03, 14, 15, 16, 17, 18, 19) and ~2.25 m (sensors: 04, 08, 09, 11, 12) above ground level. The placement of the sensors is restricted by the lounge area according EN 16798-3 [33] and inspired by ISO 7726 [34]. In consequence of this a set of decay curves is consisting out of N = 12 sensor positions in the ICC composed according to one of the two sets {01, 02, 03, 04, 05, 06, 07, 14, 15, 16, 18, 19} or {01, 02, 03, 04, 05, 06, 07, 08, 09, 11, 12, 17}. Additionally, there is one sensor in the ECC.

2.2.3. Uncertainties

The determination of the parameters ε^{a}, $\varepsilon_i^{\mathrm{a}}$ and $\varepsilon_{N,j}^{\mathrm{a}}$ includes mainly three sources of uncertainties: the uncertainty of the sensor position, the uncertainty of the measuring instruments and those resulting from the calculation method. A detailed summary of all considered uncertainties can be found in Hörberg [36].

In order to measure several physical properties for a certain volume fraction of the indoor volume it was necessary to use a set of sensors for each "point" of measurement. Around the measurement point coordinate the sensor positions varied with ±5 cm in x- and y-direction and with ±25 cm in z-direction for the sensors mounted on the stand in the middle of the room. The rest of the measurement point coordinates had a position uncertainty of ±5 cm in all directions since just one sensor each has been used.
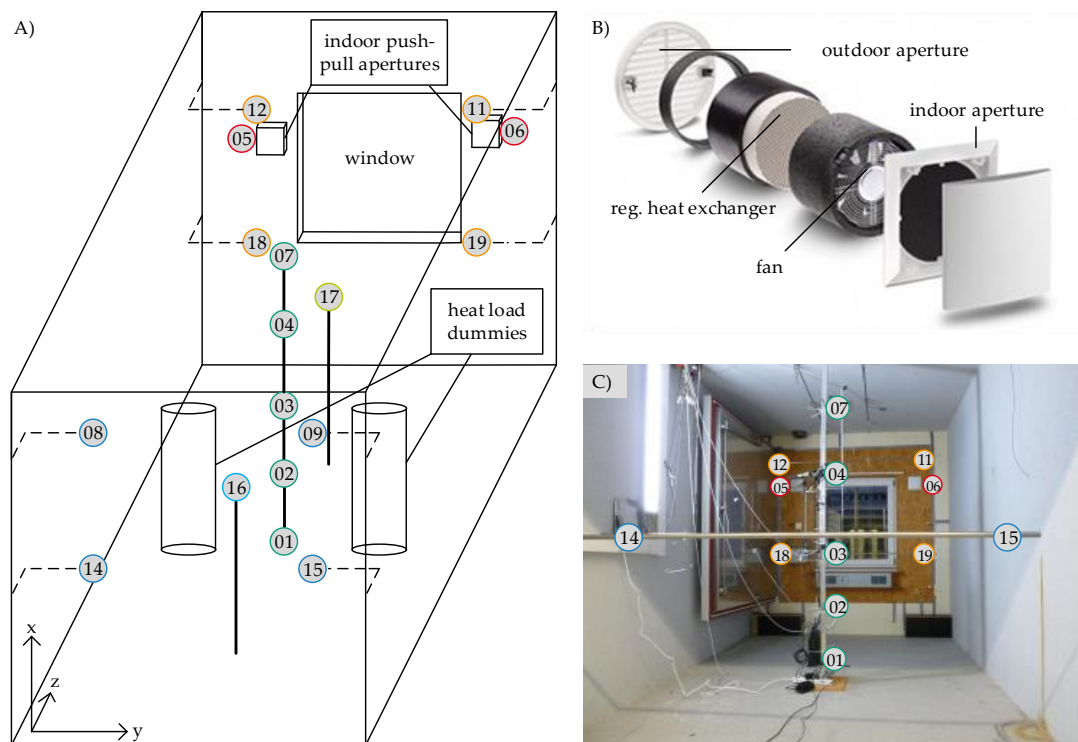
Figure 4. (**A**) Sketch: Position of the sensors in the ICC, 2.77 m × 2.70 m × 5.00 m, (**B**) Exploded view Lunos e^2 [35], (**C**) Photo of the measurement setup with some of the sensors installed and the passive house façade-model installed between the ICC and ECC.

The uncertainties of all the sensors have been reduced through a calibration. The uncertainty of the Testo CO_2-sensors increases linearly from $<\pm12$ ppm at 350 ppm till $< \pm50$ ppm at 2350 ppm and for the EnOcean CO_2-sensors from $< \pm48$ ppm at 350 ppm till $< \pm110$ ppm at 2000 ppm. The coverage factor of these uncertainties is $k_p = 2$ [37].

Rotating vane anemometers cannot accurately determine the effective volumetric air flow in alternating operation due to the associated changeover and switching times. Typical uncertainties are estimated with >5% [38]. A contributory uncertainty results from the fact that the volumetric air flow is measured upfront with a handheld device and assumed to remain the same during the air distribution measurements. The influence of changing boundary conditions is neglected.

A homogeneous initial CO_2-concentration in the entire ICC is of decisive importance for recording the decay curves. In reality, an ideal uniformity can hardly be achieved, the ranges in the measurements carried out are $R_C(t_0) < 309$ ppm. During the measuring process, the discharged CO_2 temporarily accumulates in the ECC and causes an increased concentration compared to outdoor air levels ($\overline{\Delta C}_{ECC}$ = 64 ppm). The supply of this slightly increased CO_2-concentration in the ECC-air decelerates the decay behaviour with varying intensity over time. Nevertheless, since this increase is relatively small compared to the accumulated indoor concentration the effect of the deceleration is assumed to be negligible.

3. Results

3.1. Observations with Regard to the Measurement Set-Up & Technology

An example for a measured set of decay curves is given by Figure 5 for the measurement 8, where all the characteristics and limitations of the sensors used and the resulting measurement data is visible.
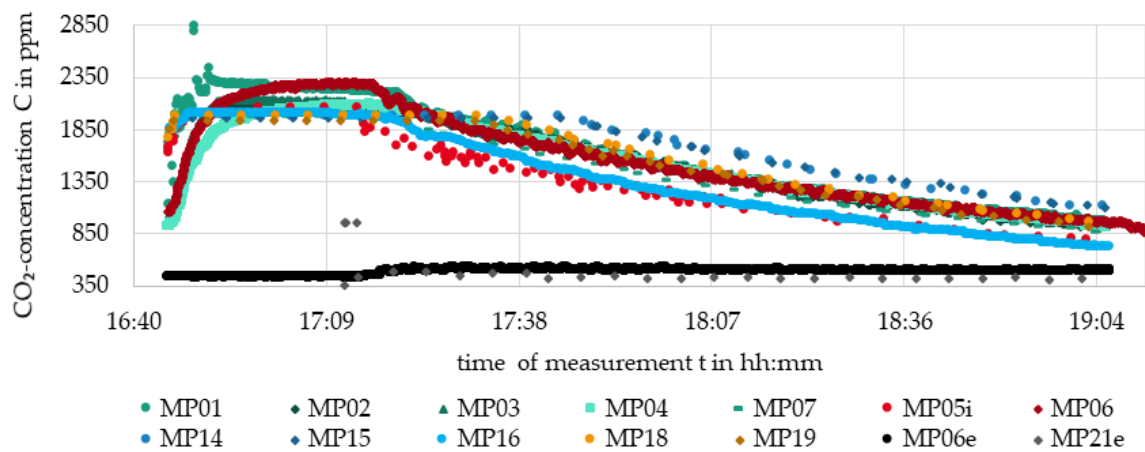
Figure 5. Example of measured decay curves: $\dot{V} = 28 \text{ m}^3 \cdot \text{h}^{-1}$, isotherm, horizontal plane at 1.10 m; the marker colours correspond to Figure 4A.

The applied low cost sensors (Afriso CO2-Sensor F) delivered data, which can be used for an evaluation. However, they have some characteristics, which need to be considered during the evaluation, for the interpretation of the results and for future measurements.

1. They cut off the concentrations >2000 ppm.
2. They measure a concentration peak during the first 2 minutes after initialisation (see MP21e)
3. They measure concentration gradients and the overall decay slope, but their maximal temporal resolution is usually not high enough for the concentration variation between supply and exhaust air phase (compare {MP01, ... ,MP04, MP06} to the others)
4. They have significant differences regarding their temporal resolution compare MP16 to the other identical sensors)
5. They are thermal hotspots, which are $\approx$ 2 °C warmer than the air around them, since they are directly powered with ~230 V. This circumstance leads to air movement influencing the air distribution.

The initial concentration has been set to $\approx$ 2000 ppm ($R_C < 250$ ppm) absolute concentration. This was sufficiently high to measure decay curves for the evaluation. Higher initial concentrations led to even more inhomogeneous initial tracer-gas distributions.

Even though the indoor air is homogenised by indoor fans (compare {MP01, MP02, MP03, MP04}) and the density of the applied tracer gas is just slightly higher compared to air, the initial concentrations decrease with increasing height. This is probably due to the cooler temperature of CO_2 during the injection.

The outdoor concentration increases after removing the caps and initialising the decay experiment. This offset in outdoor concentration has a decay behaviour as well, which leads to a damping effect of the measured indoor decay curves. The effect is stronger the closer the sensor position is to the outdoor apertures of the ventilation devices (see MP06e and MP21e).

The slope of the decay curves tends to be smaller the further away the sensor position from the push-pull devices.
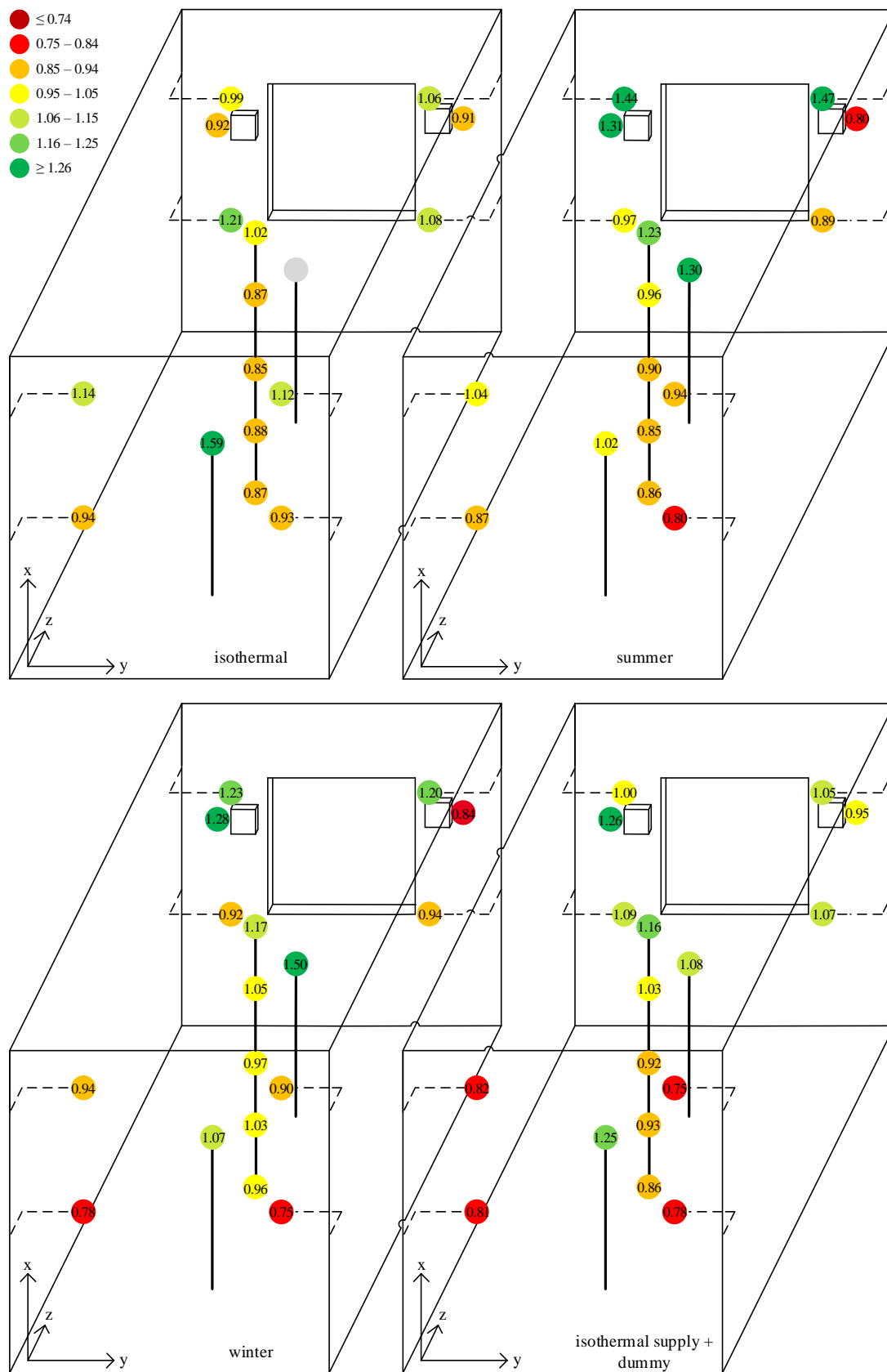
3.2. Local Air Exchange Index

The local air exchange indices $\{\varepsilon_i^a, \varepsilon_{N,j}^a\}$ are calculated based on the measured tracer gas concentration decay curves and according to the equations in the theory sections "Age of air" and "Local air exchange". The results vary within a range of $0.61 \leq \varepsilon_i^a \leq 1.12$ and $0.91 \leq \varepsilon_{N,j}^a \leq 1.34$ for the isothermal baseline measurement. The ranges of all cases in Table 4 are $0.53 \leq \varepsilon_i^a \leq 1.59$ and $0.69 \leq \varepsilon_{N,j}^a \leq 1.34$. The specific values for the investigated setups with their assigned uncertainty are shown in

Tables A1–A4 and graphically illustrated in Figure 6 ($\dot{V} = 15\ \mathrm{m^3 \cdot h^{-1}}$) and Figure 7 ($\dot{V} = 28\ \mathrm{m^3 \cdot h^{-1}}$) for a better spatial understanding.
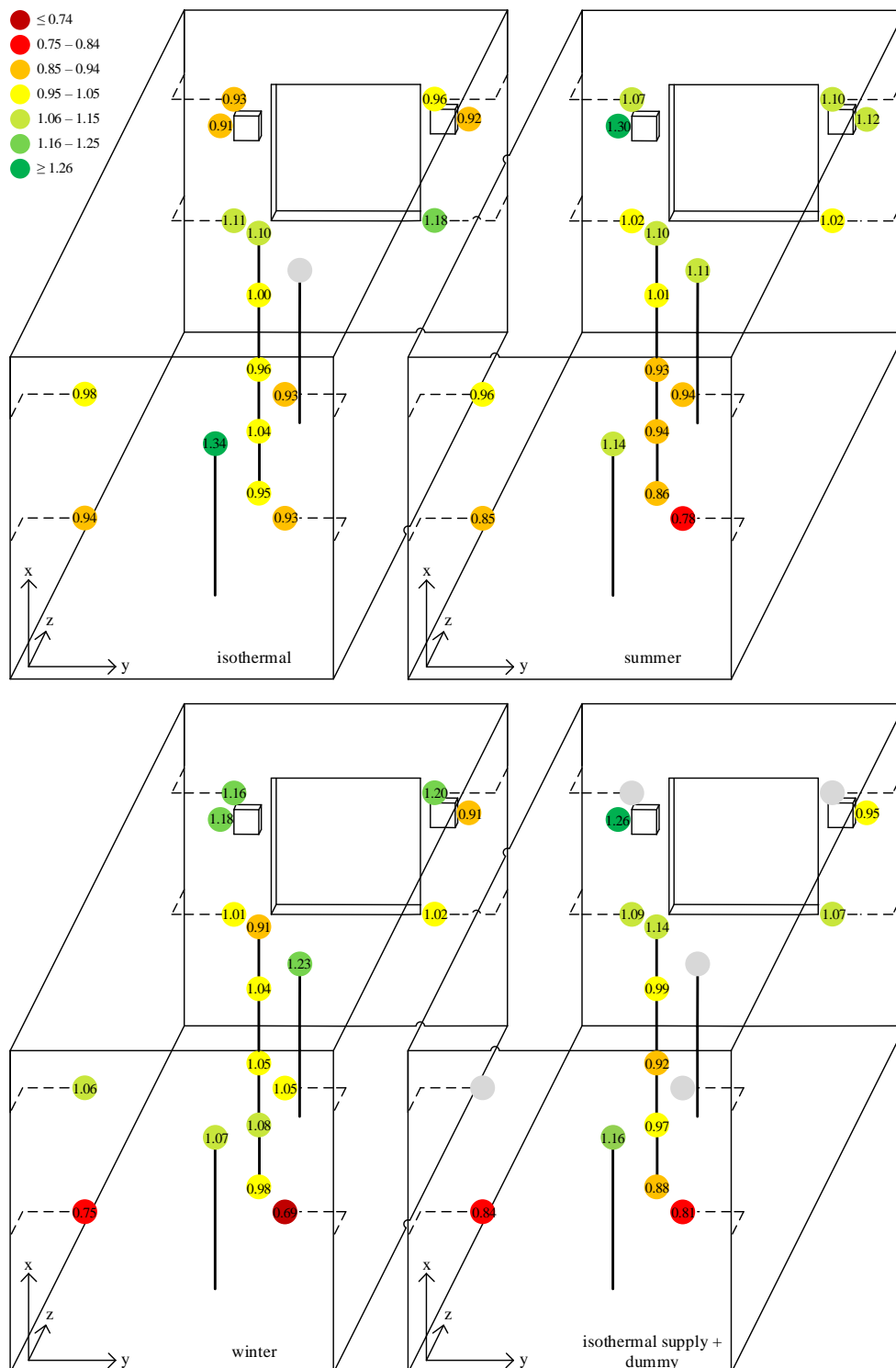
Figure 6. Local air exchange indices $\varepsilon^a_{N,j}$ (2–3) at $\dot{V} = 15\ \mathrm{m^3 \cdot h^{-1}}$: isothermal (**top left**), summer (**top right**), winter supply air conditions (bottom left), isothermal supply air conditions plus placement of a dummy to simulate human heat dissipation of 300 W (**bottom right**) [36].

Figure 7. Local air exchange indices ε^a_{Nj} (2–3) at $\dot{V} = 28$ m$^3\cdot$h^{-1}: isothermal (**top left**), summer (**top right**), winter supply air conditions (**bottom left**), isothermal supply air conditions plus placement of a dummy to simulate human heat dissipation of 300 W (**bottom right**) [36].

The grey marker in the figures had to be used in case of a lack of data either because a single sensor was not operating or because a set-up has not successfully been measured. Nevertheless, the illustrations show some interesting behaviours of the distribution of the fresh air.

First viewing from a greater distance on both setts simultaneously the set of Figure 7 appears more colourful than Figure 6. This is because the cases with a volume flow of 28 m^3 · h^{-1} had higher difference in their local air ages $\bar{\tau}_{P,i}$ and therefore the spread of the local air exchange indicators $\varepsilon^a_{N,j}$ are more distinctive.

Second, in all but one case either MP14 or MP15 had the lowest value for $\varepsilon^a_{N,j}$. As well MP08 and MP09 showed in the best case an average value. This is because the air exchange in this region of the room is not good enough.

Another interesting behaviour can be found by comparing the values of MP01, MP02, MP03, MP04 and MP07 for the summer and winter case with the isothermal case. While in summer the values of the higher positioned sensors MP04 and MP07 improve for the winter case especially MP01, MP02 & MP03 improve. If this can be found in future investigations as well this should definitely be considered in the design phase of push-pull systems, since fresh (and cold) air on the floor, in winter is certainly not a resident's desire.

Apart from this, comparing the summer and winter cases to the isothermal case it can be found that MP11 and MP12 improve over MP18 and MP19 with a temperature gradient between the in- and outdoor chambers.

The two cases including heat sources seem to be similar to the summer cases but with even higher differences for the air exchange indicators.

An odd behaviour can be found for MP16 and MP17. These sensor positions always show relatively high values for the air exchange indicators. It is not clear what the possible reasons are for this. But, since both positions are measured by the same sensor in different measurements a sensor issue seems to be plausible.

3.3. Global Air Exchange Efficiency

For the global air exchange efficiency ε^a it is also noticeable that the values for the nominal volumetric air flow acc. to [10] $\dot{V} = 28$ m^3·h^{-1} are lower than those for the smaller volumetric flow $\dot{V} = 15$ m^3·h^{-1}. Table 7 shows the mean values (horizontal plane at 1.10 m and 2.25 m) for the investigated experimental setups. The values are below the expected range $0.5 \leq \varepsilon^a \leq 1$ for almost all scenarios and thus indicate noticeable short-circuit currents. Solely in case of additional thermal convection, generated by a dummy for the emulation of human heat dissipation, the global air exchange improves up to $\varepsilon^a = 0.60$. Comparing the values of Table 7 with those of Table 2 shows that the obtained results are within the same range, however at the lower end. Almost ideal mixing ventilation, as often described in scientific literature for regenerative devices, cannot be confirmed in this series of measurements.

Table 7. Global air exchange efficiencies ε^a of various experimental setups. $\overline{\Delta\vartheta}$ is the temperature difference between the outer chamber and the inner chamber at the start of the experiment.

Supply Air	$\dot{V} = 15$ m^3·h^{-1}	$\dot{V} = 28$ m^3·h^{-1}
Isothermal	0.38 ± 0.11	0.34 ± 0.07
Warm $\left(\overline{\Delta\vartheta} = 14.3\ °C\right)$	0.50 ± 0.14	0.43 ± 0.09
Cold $\left(\overline{\Delta\vartheta} = -12.4\ °C\right)$	0.43 ± 0.11	0.35 ± 0.07
Isothermal + dummy	0.60 ± 0.15	0.41 ± 0.07

4. Discussion

Within the scope of this work, concentration decay measurements were recorded applying a combination of mainly low-cost sensors and precise sensors. This combination delivered a sufficient

data quality to be used for the calculation of the local air age $\overline{\tau}_{P,i}$ and the spatial average of air age $\langle\overline{\tau}\rangle$ at up to 14 sensor positions in the lounge space of a room plus two sensor positions at the indoor aperture of the push-pull devices. Based on these two parameters the characterisation quantities for the local air exchange {ε_i^a, $\varepsilon_{N,j}^a$} and the global air exchange efficiency ε^a are calculated. In order to interpret the results, the effects of different boundary conditions on these parameters are analysed individually below.

4.1. Effect of the Provided Air Flow Rate Level

In the investigated case, the global air exchange effectiveness ε^a decreases with higher volumetric air flow conveyed. This may be explained by the higher flow-impulse, which reduces the thermal influence by vertical buoyancy differences on the flow emitted parallel to the wall and especially the window between the two push-pull devices. With an increasing flow impulse it a larger fraction of the flow directed horizontally, towards the communicating push-pull unit - in exhaust air mode -, seems to leave the room without mixing with the indoor air. As a result of this interpretation indoor apertures with openings allowing a vertical flow direction only and a further distance between the devices are recommended for this use case.

4.2. Effect of Non-Isothermal Enclosures

Non-isothermal enclosing surfaces exchange thermal energy with the immediately adjacent air and thus cause draught. This phenomenon is most evident as downdraught in the zone near a cold window. In the present work the temperature difference between the inner surface of the window and the room air temperature is approximately 1.5 K on average. For comparison, the temperature of the wall surface deviates only by 0.2 K. The induced thermal convection was calculated to a maximum of $u_{th} = 0.15 \text{ m} \cdot \text{s}^{-1}$ by the procedure described in [36] as a summary of [39] and [40]. This is more than the average flow velocity of $u = 0.05 \text{ m} \cdot \text{s}^{-1}$ measured in the geometric centre of the room and is not negligible as an influencing factor.

4.3. Effect of Non-Isothermal Supply Air

Temperature differences between the supply air and the room air (non-isothermal case) produce buoyancy effects due to the differences in densities. The resulting additional convection is thought to cause the observed slight increase of the global air exchange efficiency from an average of 0.38 to an average of 0.50 for summer and 0.43 for winter conditions. The examination of the local air exchange indicators {ε_i^a, $\varepsilon_{N,j}^a$} reveals that improvement only occurs in parts of the room. If the supply air is introduced at elevated temperature during summer it is more likely to move in the upper part of the room, whereas the lower room volume shows better air exchange in winter. Combined with the fact that the sensors are predominantly located in the upper room volume relevant for respiration, this effect could be responsible for a better evaluation of the summer case compared to the winter case.

4.4. Effect of Human Heat Dissipation

A heat dissipation dummy (300 W) was positioned halfway between the façade equipped with the push-pull and the opposite unequipped room side. The dummy simulates the human heat dissipation and generates an additional vertical convection current. This causes the global air exchange efficiency to rise to a value of $\varepsilon^a > 0.5$ typical for displacement ventilation. The increase is primarily reflected in higher local air exchange {ε_i^a, $\varepsilon_{N,j}^a$} ratings in the front part of the room, whereas the room volume further away from the ventilation units is rather insufficiently ventilated (Figures 6 and 7, low right). The greater spatial inhomogeneity is reflected in a range enlarged to $0.81 \le \varepsilon_{N,j}^a \le 1.32$ ($R_{\varepsilon_{N,j}^a} = 0.51$) compared with $R_{\varepsilon_{N,j}^a} = 0.41$ in the isothermal case.

5. Conclusions

A preliminary laboratory investigation regarding the ventilation effectiveness based on the air exchange efficiency was carried out in a climatic chamber. The combination of an outdoor and indoor climate chamber separated by a passive house façade model is representing a single room equipped with two alternating façade-integrated ventilation devices with regenerative heat recovery. The measurements have been carried out applying a cost-effective set-up, which is accepted by residents of real houses. These preliminary test show that such a set-up can be applied for air exchange evaluations. Based on the experience of this laboratory measurements, this method and measurement set-up appears to be suitable for field measurement campaigns regarding the air exchange efficiency of buildings equipped with push-pull devices under varying climate and weather conditions.

The results show that the sole indication of the volumetric air flow rate conveyed by push-pull ventilation units is not sufficient for the evaluation of the effective air renewal in the room. The air exchange efficiency varies with changes in the boundary conditions such as airflow rate, outside air temperature and internal heat sources. Whilst the isothermal baseline measurement falls significantly below the expected range of air exchange efficiency ($0.5 \leq \varepsilon^a \leq 1$), thus indicating potential ventilation shortcuts, the air exchange efficiency increases to a maximum of $\varepsilon^a = 0.6$ with additional thermal convection in the case of a heat dissipating source in the room. Other than initially assumed, mixing ventilation can not be observed for most cases, but a spatially inhomogeneous distribution with pronounced short-circuiting currents are indicated by the measurement results. The installation of both ventilation units in the same façade side as specified in the climate chamber does not seem optimal. Further distance between the communicating ventilation units and apertures assuring a vertical flow direction are assumed to improve air exchange efficiency. Further research is therefore also required on the placement of domestic ventilation units in the room.

Nomenclature

Dimensions			**Indexes & Operators** [41]	
C	CO$_2$-concentration	ppm	da	dry air
R	range	-	ma	moist air
n	air exchange rate	-	e	exhaust air
t	time	s	i	local point i in space
T	temperature	K	j	local point j in space
u	velocity	$m \cdot s^{-1}$	$\bar{\cdot}$	time average
ε^c	contaminant removal	-	$\langle \cdot \rangle$	spacial average
ε^a	air exchange efficiency	-	P	probe
η_T	heat recovery rate	%	N	nummer of sensors
φ	relative humidity	%rh	exh	exhaust
ρ	density	$kg \cdot m^{-3}$	sup	supply
ϑ	temperature	°C	out	outdoor
τ	air age	s	$[\cdot, \cdot]$	entire closed interval
τ_{nom}	nominal time const.	s	$\forall$	for all
$\dot{V}$	volume flow	$m^3 \cdot h^{-1}$	$\in$	element of
X	absolute humidity	$g(H_2O) \cdot kg(da)^{-1}$	$\wedge$	logical and
M	molar mass	$kg^3 \cdot mol^{-1}$	$|\cdot|$	number of elements

Appendix A

Table A1. Local air exchange at unaffected (isothermal) supply air conditions.

Position	$\dot{V} = 15\ m^3 \cdot h^{-1}$		$\dot{V} = 28\ m^3 \cdot h^{-1}$	
	ε_i^a in -	$\varepsilon_{N,j}^a$ in -	ε_i^a in -	$\varepsilon_{N,j}^a$ in -
01	0.73 ± 0.02	0.95 ± 0.11	0.61 ± 0.02	0.87 ± 0.16
02	0.79 ± 0.02	1.04 ± 0.10	0.62 ± 0.02	0.88 ± 0.16
03	0.73 ± 0.02	0.96 ± 0.10	0.60 ± 0.02	0.85 ± 0.16
04	0.76 ± 0.02	1.00 ± 0.10	0.61 ± 0.02	0.87 ± 0.16
05	0.69 ± 0.02	0.91 ± 0.11	0.65 ± 0.02	0.92 ± 0.15
06	0.70 ± 0.02	0.92 ± 0.11	0.64 ± 0.02	0.91 ± 0.15
07	0.84 ± 0.03	1.10 ± 0.09	0.72 ± 0.02	1.02 ± 0.14
08	0.75 ± 0.03	0.98 ± 0.10	0.69 ± 0.02	0.98 ± 0.15
09	0.71 ± 0.03	0.93 ± 0.11	0.63 ± 0.02	0.90 ± 0.15
10	0.71 ± 0.03	0.93 ± 0.11	0.70 ± 0.02	0.99 ± 0.15
11	0.74 ± 0.03	0.96 ± 0.10	0.75 ± 0.02	1.06 ± 0.14
14	0.72 ± 0.03	0.94 ± 0.11	0.80 ± 0.02	1.14 ± 0.13
15	0.71 ± 0.03	0.93 ± 0.11	0.79 ± 0.02	1.12 ± 0.13
16	1.02 ± 0.03	1.34 ± 0.08	1.12 ± 0.02	1.59 ± 0.11
17	-	-	-	-
18	0.84 ± 0.03	1.11 ± 0.09	0.85 ± 0.02	1.21 ± 0.13
19	0.90 ± 0.03	1.18 ± 0.09	0.76 ± 0.02	1.08 ± 0.14
R	0.33	0.43	0.52	0.74
σ	0.09	0.11	0.13	0.18

Table A2. Local air exchange at warm supply air conditions.

Position	$\dot{V} = 15\ m^3 \cdot h^{-1}$		$\dot{V} = 28\ m^3 \cdot h^{-1}$	
	ε_i^a in -	$\varepsilon_{N,j}^a$ in -	ε_i^a in -	$\varepsilon_{N,j}^a$ in -
01	0.87 ± 0.02	0.86 ± 0.08	0.74 ± 0.02	0.86 ± 0.13
02	0.95 ± 0.02	0.94 ± 0.07	0.74 ± 0.02	0.85 ± 0.13
03	0.94 ± 0.02	0.93 ± 0.07	0.78 ± 0.02	0.90 ± 0.13
04	1.01 ± 0.02	1.01 ± 0.07	0.82 ± 0.02	0.96 ± 0.12
05	1.31 ± 0.02	1.30 ± 0.06	1.13 ± 0.02	1.31 ± 0.10
06	1.13 ± 0.02	1.12 ± 0.06	0.69 ± 0.02	0.80 ± 0.13
07	1.11 ± 0.03	1.10 ± 0.07	1.06 ± 0.02	1.23 ± 0.11
08	0.96 ± 0.03	0.96 ± 0.07	0.90 ± 0.02	1.04 ± 0.11
09	0.95 ± 0.03	0.94 ± 0.07	0.81 ± 0.02	0.94 ± 0.12
10	1.08 ± 0.03	1.07 ± 0.07	1.24 ± 0.02	1.44 ± 0.10
11	1.11 ± 0.03	1.10 ± 0.06	1.26 ± 0.02	1.47 ± 0.10
14	0.85 ± 0.03	0.85 ± 0.07	0.75 ± 0.02	0.87 ± 0.13
15	0.79 ± 0.03	0.78 ± 0.08	0.68 ± 0.02	0.80 ± 0.14
16	1.15 ± 0.03	1.14 ± 0.06	0.88 ± 0.02	1.02 ± 0.12
17	1.12 ± 0.03	1.11 ± 0.06	1.12 ± 0.02	1.30 ± 0.11
18	1.03 ± 0.03	1.02 ± 0.07	0.84 ± 0.02	0.97 ± 0.12
19	1.03 ± 0.03	1.02 ± 0.07	0.77 ± 0.02	0.89 ± 0.13
R	0.52	0.52	0.58	0.67
σ	0.13	0.12	0.19	0.22

Table A3. Local air exchange at cold supply air conditions.

Position	$\dot{V} = 15\ m^3 \cdot h^{-1}$		$\dot{V} = 28\ m^3 \cdot h^{-1}$	
	ε_i^a in -	$\varepsilon_{N,j}^a$ in -	ε_i^a in -	$\varepsilon_{N,j}^a$ in -
01	0.84 ± 0.02	0.98 ± 0.08	0.68 ± 0.02	0.96 ± 0.14
02	0.92 ± 0.02	1.08 ± 0.07	0.73 ± 0.02	1.03 ± 0.13
03	0.90 ± 0.02	1.05 ± 0.07	0.69 ± 0.02	0.97 ± 0.14
04	0.89 ± 0.02	1.04 ± 0.07	0.74 ± 0.02	1.05 ± 0.13
05	1.10 ± 0.02	1.18 ± 0.07	0.91 ± 0.02	1.28 ± 0.12
06	0.78 ± 0.02	0.91 ± 0.08	0.60 ± 0.02	0.84 ± 0.15
07	0.78 ± 0.03	0.91 ± 0.08	0.83 ± 0.02	1.17 ± 0.12
08	0.90 ± 0.03	1.06 ± 0.07	0.66 ± 0.02	0.94 ± 0.14
09	0.90 ± 0.03	1.05 ± 0.07	0.64 ± 0.02	0.90 ± 0.15
10	0.99 ± 0.03	1.16 ± 0.07	0.87 ± 0.02	1.23 ± 0.12
11	1.03 ± 0.03	1.20 ± 0.07	0.85 ± 0.02	1.20 ± 0.12
14	0.64 ± 0.03	0.75 ± 0.07	0.55 ± 0.02	0.78 ± 0.16
15	0.59 ± 0.03	0.69 ± 0.10	0.53 ± 0.02	0.75 ± 0.17
16	0.92 ± 0.03	1.07 ± 0.07	0.78 ± 0.02	1.10 ± 0.13
17	1.05 ± 0.03	1.23 ± 0.07	1.06 ± 0.02	1.50 ± 0.11
18	0.86 ± 0.03	1.01 ± 0.08	0.65 ± 0.02	0.92 ± 0.15
19	0.87 ± 0.03	1.02 ± 0.08	0.66 ± 0.02	0.94 ± 0.14
R	0.46	0.54	0.53	0.75
σ	0.12	0.14	0.13	0.19

Table A4. Local air exchange at unaffected supply air conditions + internal heat source of 300 W.

Position	$\dot{V} = 15$ m$^3 \cdot$h^{-1}		$\dot{V} = 28$ m$^3 \cdot$h^{-1}	
	ε_i^a in -	$\varepsilon_{N,j}^a$ in -	ε_i^a in -	$\varepsilon_{N,j}^a$ in -
01	1.06 ± 0.02	0.88 ± 0.05	0.71 ± 0.02	0.86 ± 0.12
02	1.17 ± 0.02	0.97 ± 0.05	0.76 ± 0.02	0.93 ± 0.12
03	1.11 ± 0.02	0.92 ± 0.05	0.75 ± 0.02	0.92 ± 0.12
04	1.19 ± 0.02	0.99 ± 0.05	0.84 ± 0.02	1.03 ± 0.11
05	1.59 ± 0.02	1.32 ± 0.04	1.03 ± 0.02	1.26 ± 0.10
06	1.25 ± 0.02	1.04 ± 0.05	0.78 ± 0.02	0.95 ± 0.12
07	1.37 ± 0.03	1.14 ± 0.05	0.95 ± 0.02	1.16 ± 0.11
08	-	-	0.67 ± 0.02	0.82 ± 0.13
09	-	-	0.62 ± 0.02	0.75 ± 0.14
10	-	-	0.82 ± 0.02	1.00 ± 0.11
11	-	-	0.86 ± 0.02	1.05 ± 0.11
14	1.01 ± 0.03	0.84 ± 0.06	0.67 ± 0.02	0.81 ± 0.13
15	0.97 ± 0.03	0.81 ± 0.05	0.64 ± 0.02	0.78 ± 0.13
16	1.40 ± 0.03	1.16 ± 0.05	1.03 ± 0.02	1.25 ± 0.10
17	-	-	0.88 ± 0.02	1.08 ± 0.11
18	1.28 ± 0.03	1.07 ± 0.05	0.89 ± 0.02	1.09 ± 0.11
19	1.29 ± 0.03	1.07 ± 0.05	0.87 ± 0.02	1.07 ± 0.11
R	0.62	0.51	0.41	0.51
σ	0.17	0.14	0.12	0.15

References

1. Bundesverband der Deutschen Heizungsindustrie e., V. Entwicklung Wärmemarkt Deutschland 2019; Köln. Available online: www.bdh-koeln.de/fileadmin/user_upload/Pressemeldungen/Marktentwicklung_Waermemarkt_2019.pdf (accessed on 13 July 2020).
2. Maurer, K. Warum die Wohnraumlüftung bei der Planung oft unter den Tisch fällt. Available online: https://www.haustec.de/klima-lueftung/lueftungstechnik/warum-die-wohnraumlueftung-bei-der-planung-oft-unter-den-tisch?page=all. (accessed on 29 October 2020).
3. Bundesverband der Deutschen Heizungsindustrie e., V. Marktentwicklung Wärmemarkt Deutschland 2018; Köln. Available online: www.bdh-koeln.de/fileadmin/user_upload/Marktentwicklung_Deutschland_2018.pdf (accessed on 13 July 2020).
4. Bundesverband der Deutschen Heizungsindustrie e., V. Marktentwicklung Wärmemarkt Deutschland 2017; Köln. Available online: www.bdh-koeln.de/fileadmin/user_upload/pressemitteilungen_pdf/Marktentwicklung_Waermemarkt_2017.pdf (accessed on 22 June 2018).
5. Maier, D. Aufbau und Durchführung einer Mixed-Methods-Studie zu Lüftungsverhalten und Raumklima sowie der Einstellung bezüglich Lüftungssystemen. Master's Thesis, Katholische Universität Eichstätt-Ingolstadt, Eichstätt, Ingolstadt, 2020.
6. Manz, H.; Huber, H.; Schälin, A.; Weber, A.; Ferrazzini, M.; Studer, M. Performance of single room ventilation units with recuperative or regenerative heat recovery. *Energy Build.* **2000**, *31*, 37–47. [CrossRef]
7. *Delegierte Verordnung (EU), Nr. 1254/2014 der Komission—Vom 11. Juli 2014—Zur Ergänzung der Richtlinie 2010/30/EU des Europäischen Parlaments und des Rates im Hinblick auf die Kennzeichnung von Wohnraumlüftungsgeräten in Bezug auf den Energieverbrauch: EU 1254/2014.*; EUR-Lex Access to European Union Law: Brussels, Belgium, 2014; pp. 27–45.
8. Merzkirch, A. Energieeffizienz, Nutzerkomfort und Kostenanalyse von Lüftungsanlagen in Wohngebäuden: Feldtests von neuen Anlagen un Vorstellung bedarfsgeführter Prototypen. Ph.D. Thesis, University of Luxembourg, Luxemburg, 2015.
9. Mathis, P.D.-I.; Röder, T.S.; Klein, B.D.-I.; Hartmann, T.D.-I.; Knaus, C.D.-I. EwWalt—Energetische Bewertung der dezentralen kontrollierten Wohnraumlüftung in alternierender Betriebsweise. Abschlussbericht. Aktenzeichen SWD-10.08.18.7-16.32; TGA Report. 2019. Available online: https://downloads.fgk.de/335_TGA-Report_06_EwWalt.pdf (accessed on 8 July 2019).

10. Deutsches Institut für Normung, e.V. *Raumlufttechnik—Teil 6: Lüftung von Wohnungen—Allgemeine Anforderungen, Anforderungen an die Auslegung, Ausführung, Inbetriebnahme und Übergabe sowie Instandhaltung*; Beuth Verlag GmbH: Berlin, Germany, 2019; 91.140.30 (1946-6). [CrossRef]

11. LUNOS. Lüftungstechnik GmbH für Raumluftsysteme. *Technisches Infoblatt. Lüftung mit Wärmerückgewinnung—e²Einschub.* 2016. Available online: www.lunos.de (accessed on 10 July 2020).

12. Merckx, M.; Bruyneel, G.; Laverge, J.; Pollet, I. Temperature, draft and ventilation efficiency of room based decentralised heat recovery ventilation systems. In Proceedings of the Smart Ventilation for buildings 39th AIVC Conference 7th TightVent Conference 5th Venticool ConferenceSepember 2018, Antibes Juan-Les-Pins, France, 18–19 September 2018; Air Infiltration and Ventilation Centre, Venticool—The International Platform for Ventilative Cooling, TightVent Europe—Building and Ductwork Airtightness Platform, Eds. Available online: www.aivc.org/resource/temperature-draft-and-ventilation-efficiency-room-based-decentralised-heat-recovery (accessed on 22 October 2018).

13. Cui, S.; Cohen, M.; Stabat, P.; Marchio, D. CO2 tracer gas concentration decay method for measuring air change rate. *Build. Environ.* **2015**, *84*, 162–169. [CrossRef]

14. Sandberg, M. What is ventilation efficiency? *Build. Environ.* **1981**, *16*, 123–135. [CrossRef]

15. Deutsches Institut für Normung, e.V.; International Organization for Standardization. *Innenraumluftverunreinigungen—Teil 8: Bestimmung des lokalen Alters der Luft in Gebäuden zur Charakterisierung der Lüftungsbedingungen (ISO 16000-8:2007)*; Beuth Verlag GmbH: Berlin, Germany, 2008. Available online: https://www.beuth.de/de/norm/din-iso-16000-8/102342071 (accessed on 18 May 2018). [CrossRef]

16. Goodwin, E.T. The evaluation of integrals of the form. *Math. Proc. Camb. Phil. Soc.* **1949**, *45*, 241–245. [CrossRef]

17. Mundt, E.; Mathisen, H.M.; Nielsen, P.V.; Moser, A. *Ventilation Effectiveness*; Rehva: Brussels, Belgium, 2004; ISBN 9782960046809.

18. Roulet, C.-A.; Vandaele, L. *Air Flow Patterns within Buildings, Measurement Techniques. Air Leakage Measurement Methods, Air flow Measurement Methods, Measurement Methods Related to Efficiency, Measurements on Ventilation Systems. Technical Note AIVC 34*; Air Infiltration and Ventilation Centre: Coventry, Great Britain, 1991; ISBN 0946075646.

19. Maas, A. Experimentelle Quantifizierung des Luftwechsels bei Fensterlüftung. Ph.D. Thesis, Universität Gesamthochschule Kassel, Kassel, Germany, 1995.

20. Sandberg, M. Prof. Ph.D (Eng). The Multi-chamber Theory Reconsidered from the Viewpoint of Air Quality Studies // The multi-chamber theory reconsidered from the viewpoint of air quality studies. *Build. Environ.* **1984**, *19*, 221–233. [CrossRef]

21. International Organization for Standardization; European Committee for Standardization; Deutsches Institut für Normung e.V. *Wärmetechnisches Verhalten von Gebäuden und Werkstoffen—Bestimmung des Spezifischen Luftvolumenstroms in Gebäuden—Indikatorgasverfahren (ISO 12569:2017); Deutsche Fassung EN ISO 12569:2017*, 1st ed.; Beuth Verlag GmbH: Berlin, Germany, 2018; 91.120.10 (12569). [CrossRef]

22. Skaaret, E. Contaminant removal performance in terms of ventilation effectiveness. *Environ. Int.* **1986**, *12*, 419–427. [CrossRef]

23. Novoselac, A.; Srebric, J. Comparison of Air Exchange Efficiency and Contaminant Removal Effectiveness as IAQ Indices. *ASHRAE Trans.* **2003**. Available online: www.caee.utexas.edu/prof/novoselac/Publications/Novoselac_ASHRAE_Transactions_2003.pdf (accessed on 29 October 2020).

24. Kuber, T. Energy Evaluation of Decentralized Ventilation Systems. Master's Thesis, Hochschule Offenburg, Offenburg, Germany, 2014.

25. Testo SE & Co. KGaA. CO2 probe—CO2 probe: Order-Nr. 0632 1240. Available online: https://www.testo.com/en-US/co2-probe/p/0632-1240 (accessed on 12 October 2020).

26. Testo SE & Co. KGaA. Standard Humidity/Temperature Probe (Ø 21 mm): Order-Nr. 0636 9740. Available online: https://www.testo.com/en-SG/standard-ambient-air-probe-up-to-70degc/p/0636-9740 (accessed on 13 October 2020).

27. Testo SE & Co. KGaA. Comfort Level Probe for Measuring Degree of Turbulence, with Telescopic Handle and Stand. Fulfills EN 13779 requirements: Order-Nr. 0628 0009. Available online: https://www.testo.com/en-TH/comfort-level-probe-for-measuring-degree-of-turbulence-with/p/0628-0009 (accessed on 12 October 2020).

28. Thermokon Sensortechnik GmbH EasySens®–Transmitter–Humidity–SR65 rH. Available online: www.thermokon.de/en/products/easysensr-transmitter/humidity/sr65-rh/ (accessed on 12 October 2020).

29. Testo SE & Co. KGaA. Temperature Probe Ø 12 mm: Order-Nr. 0636 9743. Available online: https://www.testo.com/en-IN/temperature-probe-o-12-mm/p/0636-9743 (accessed on 12 October 2020).

30. Testo SE & Co. KGaA. IAQ probe including tripod: Order-Nr. 0632 1543. Available online: https://www.testo.com/en-US/iaq-probe-including-tripod/p/0632-1543 (accessed on 12 October 2020).

31. Testo SE & Co. KGaA. Comfort Level Probe: Order-Nr. 0628 0143. Available online: https://www.testo.com/en-US/comfort-level-probe/p/0628-0143 (accessed on 12 October 2020).

32. Afriso Euro Index GmbH. Datenblatt—CO2-Sensor. 2020. Available online: https://www.afriso.com/ix_pim_assets/PDF/6/86/286/CO2-Sensor-DB.pdf (accessed on 13 October 2020).

33. Deutsches Institut für Normung, e.V.; European Committee for Standardization. *Energetische Bewertung von Gebäuden – Lüftung von Gebäuden—Teil 3: Lüftung von Nichtwohngebäuden—Leistungsanforderungen an Lüftungs- und Klimaanlagen und Raumkühlsysteme (Module M5-1, M5-4); Deutsche Fassung EN 16798-3:2017*, 1st ed.; Beuth Verlag GmbH: Berlin, Germany, 2017; 16798-3 (16798-3). Available online: http://perinorm-fr.redi-bw.de/volltexte/CD21DE14/2596017/2596017.pdf? (accessed on 19 February 2019). [CrossRef]

34. Deutsches Institut für Normung, e.V.; European Committee for Standardization; International Organization for Standardization. *Umgebungsklima Instrumente zur Messung physikalischer Größen (ISO 7726:1998) Deutsche Fassung EN ISO 7726:2001. DIN EN ISO 7726*, 1st ed.; Beuth Verlag GmbH: Berlin, Germany, 2002; 13.040.20 (7726). Available online: http://fhgonline.fhg.de/bibliotheken/ise/DIN_EN_ISO_7726_April_2002.pdf (accessed on 1 September 2017).

35. LUNOS. Lüftungstechnik GmbH für Raumluftsysteme. e^2 mit Wärmerückgewinnung: Kontrollierte Wohnungslüftung mit dem e^2 mit Wärmerückgewinnung. Available online: https://www.lunos.de/alle-produkte/e%C2%B2 (accessed on 10 July 2020).

36. Hörberg, C. Lüftungswirksamkeit und hygrothermische Behaglichkeit von alternierend arbeitenden fassadenintegrierten Lüftungsgeräten. Master's Thesis, Hochschule Biberach, Biberach, Germany, 2019.

37. International Electrotechnical Commission. Uncertainty of Measurement Part 3: Guide to the Expression of Uncertainty in Measurement (GUM:1995), 2011 (98-3 Supplement 2). Available online: www.iso.org/standard/50461.html (accessed on 18 May 2018).

38. Klein, B.D.-I.; Siebler, L. Prüfverfahren für dezentrale alternierende Wohnungslüftungsgeräte. *HLH* **2018**, *69*, 33–36.

39. Schmidt, E.; Beckmann, W. Das Temperatur- und Geschwindigkeitsfeld vor einer Wärme abgebenden senkrechten Platte bei natürlicher Konvektion. *Tech. Mech. und Thermodyn.* **1930**, 391–406. [CrossRef]

40. Holman, J.P. *Heat Transfer*, 10th ed.; McGraw-Hill; McGraw Hill Higher Education: New York, NY, USA, 2010; ISBN 978-0-07-352936-3.

41. Deutsches Institut für Normung, e.V.; European Committee for Standardization; International Organization for Standardization. *Größen und Einheiten—Teil 2: Mathematik (ISO 80000-2:2019); Deutsche Fassung EN ISO 80000-2:2019*, 1st ed.; Beuth Verlag GmbH: Berlin, Germany, 2020; 01.060; 01.075 (80000-2). [CrossRef]

Publisher's Note: MDPI stays neutral with regard to jurisdictional claims in published maps and institutional affiliations.